Optics Letters

Optical nonlinearities in high-confinement silicon carbide waveguides

Jaime Cardenas,[1] Mengjie Yu,[2] Yoshitomo Okawachi,[2] Carl B. Poitras,[1] Ryan K. W. Lau,[2] Avik Dutt,[1] Alexander L. Gaeta,[2,3] and Michal Lipson[1,3,*]

[1]School of Electrical and Computer Engineering, Cornell University, Ithaca, New York 14853, USA
[2]School of Applied Engineering Physics, Cornell University, Ithaca, New York 14853, USA
[3]Kavli Institute at Cornell for Nanoscale Science, Cornell University, Ithaca, New York 14853, USA
*Corresponding author: lipson@ece.cornell.edu

Received 25 May 2015; revised 5 August 2015; accepted 9 August 2015; posted 11 August 2015 (Doc. ID 241540); published 31 August 2015

We demonstrate strong nonlinearities of $n_2 = 8.6 \pm 1.1 \times 10^{-15}$ cm^2 W^{-1} in single-crystal silicon carbide (SiC) at a wavelength of 2360 nm. We use a high-confinement SiC waveguide fabricated based on a high-temperature smart-cut process.

OCIS codes: (130.3120) Integrated optics devices; (190.4390) Nonlinear optics, integrated optics.

http://dx.doi.org/10.1364/OL.40.004138

The past decade has seen tremendous developments in complementary metal-oxide semiconductor (CMOS)-compatible platforms for integrated nonlinear optical devices, including silicon (Si), high-index glass (Hydex), silicon nitride (Si_3N_4), aluminum nitride, and diamond [1–4]. However, none of these platforms combine a large bandgap, a bulk second-order $\chi^{(2)}$ susceptibility, a high third-order $\chi^{(3)}$ susceptibility, and a high refractive index. The combination of these characteristics could enable novel functionalities on chip. The large bandgap enables photonic structures operating at visible wavelengths, while a $\chi^{(2)}$ susceptibility and a high $\chi^{(3)}$ susceptibility enable electro-optic control and optical parametric processes. The large index contrast between a waveguide core and cladding enables high confinement of the optical mode, which allows for large flexibility in dispersion engineering and makes it possible to extend the anomalous dispersion, which is essential for phase-matched nonlinear optical processes, into the mid-infrared regime [5].

Silicon carbide (SiC) is an extremely promising photonic material that has large second- and third-order nonlinearities, with $d_{33} = -14.4$ pm/V and a nonlinear refractive index of $n_2 = 1.1 \times 10^{-13}$ cm^2/W (6H SiC at 694 nm) [6], which is comparable to Si at 1550 nm [7]. Unlike Si, SiC, with its large bandgap of 2.4–3.2 eV, does not suffer from two-photon absorption at near-infrared wavelengths. In addition, its linear refractive index of $n = 2.6$ at 1550 nm is extremely high, enabling ultra-high confinement waveguides. These factors make SiC a promising platform for nonlinear photonics in both the near- and mid-infrared regions.

SiC has over 200 polytypes of different crystalline structures. The three main polytypes are 3C (cubic, T_d^2 space group), 4H (hexagonal C_{6v}^4, space group), and 6H (hexagonal C_{6v}^4, space group) with bandgaps of 2.4, 3.2, and 3.0 eV, respectively. 3C SiC is available commercially in epitaxially grown films on silicon. 4H and 6H are commercially available only as bulk crystalline wafers cut in on-axis or off-axis orientations. Since 4H and 6H SiC are uniaxial crystals, the on-axis orientation cut results in a wafer with the optical axis (c-axis of the crystal) perpendicular to its surface, with the ordinary refractive index in the plane of the wafer (extraordinary refractive index perpendicular to the plane of the wafer). This cut is ideal for photonic devices since the TE polarization aligns with the ordinary axes of the crystal and the TM polarization aligns with the extraordinary axis, thereby preventing unwanted polarization rotation.

Recently, there has been progress in the development of SiC [8–13]; however, most recent works on SiC photonic channel waveguides have been based on epitaxially grown 3C SiC, which fundamentally has a relatively high intrinsic loss. 3C SiC epitaxially grown on a silicon substrate exhibits stacking defects due to the lattice mismatch between SiC and silicon. These defects have been shown to be electrically active [14] and will lead to absorption losses within the material. Previous works in epitaxial 3C SiC have demonstrated propagation loss on the order of 35 dB/cm and, more recently, a quality factor around 50,000, which is equivalent to propagation losses on the order of 13 dB/cm [12,13]. However, these values approach the material limitation.

Here, based on bulk 4H SiC with a low intrinsic loss, we show an integrated photonic waveguide structure and its potential for nonlinear optics. Bulk SiC wafers (4H and 6H) have the highest purity and crystal quality. We estimate the upper bound on the intrinsic material losses of our bulk 4H SiC wafer (Norstel: high purity, on-axis, semi-insulating, resistivity $>1 \times 10^7$ Ohm-cm 4H 75 mm wafer) is 0.3 dB/cm by placing the SiC wafer in a high finesse cavity ($F \approx 300$) and characterizing its effect on the cavity's resonance. In contrast to epitaxially grown 3C SiC on silicon photonic structures, which consist of thin, high-confinement layers of SiC suspended in air

[13], bulk SiC requires processing in order to be useful for a photonic platform. Here, we form such a platform by using a smart-cut technique [10] to create an optically thin (<1100 nm) single crystal-on-insulator. The process flow starts by depositing 100 nm of low-pressure chemical vapor deposition (LPCVD) silicon oxide on a 3-inch, high-resistivity 4H SiC wafer. Hydrogen is implanted at 190 keV into the oxide-covered face of the wafer, which is kept at 200°C. We grow 3 μm of silicon oxide on a silicon wafer and bond it to the SiC wafer. To ensure a high-quality bond, we first polish the LPCVD oxide on the SiC wafer using a Rodel Politex Supreme pad to reduce the roughness of the deposited oxide. Both wafers undergo a "reverse" RCA clean (acid bath followed by alkaline bath) to prepare the oxide surfaces for bonding. The two wafers are manually bonded by placing the two oxide surfaces together and applying manual pressure. The bonded wafers are then annealed at 900°C to separate the thin SiC slice from the substrate (Fig. 1). The thin SiC film is polished using a Rodel IC1400 pad and Cabot Microelectronics SiCceed SiC polishing slurry. We successfully transfer a SiC film over 60% of the 3-inch wafer [top portion of the wafer in Fig. 2(a)]. The remaining area (bottom portion of the wafer) did not transfer due to defects that emerged during the bonding step. We estimate that by optimizing the polishing of the LPCVD oxide, full wafers can be transferred using this technique.

In order to minimize possible losses introduced during the processing, particularly during the implantation step, defects in the crystal structure are minimized by performing the ion implantation at a high temperature. This high temperature implantation is needed since in contrast to silicon-on-insulator, where ion implantation damage is repaired by annealing at temperatures compatible with the buried oxide, crystal repair in SiC requires annealing at temperatures in excess of 1300°C, beyond the compatibility of the buried oxide. We model

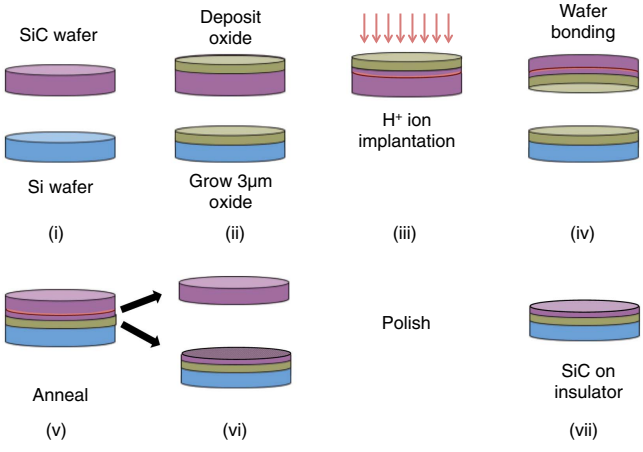

Fig. 1. Smart-cut process: the process starts from a bulk crystalline 4-H SiC wafer and a silicon wafer (i). 100 nm of LPCVD high-temperature oxide is deposited on the SiC, and 3 μm of oxide is thermally grown on the silicon wafer (ii). Next, the SiC undergoes ion implantation at 190 keV (iii). The deposited oxide on the SiC wafer is polished, and the two wafers are bonded (iv). The bonded wafers are then annealed at 900°C (v) where they split into an SiC wafer and an oxide-coated silicon wafer with a thin layer of crystalline SiC (vi). After polishing the SiC-on-insulator, the wafer is ready for device fabrication (vii).

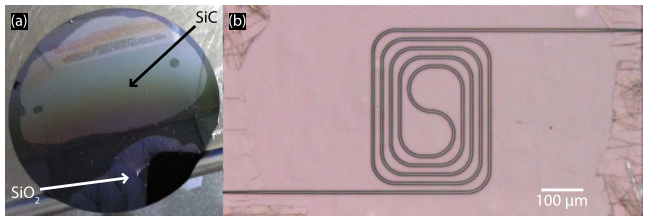

Fig. 2. (a) Photograph of a 3-inch SiC-on-insulator wafer fabricated using the smart-cut technique. The top ~60% of the wafer shows a successfully transferred film of SiC onto the oxide-covered silicon wafer. (b) Micrograph of high-confinement SiC waveguide.

the damage induced in the crystal lattice using the Athena module of Silvaco [15]. The simulations show that the damage to the crystal lattice is strongly dependent on the sample temperature during implantation (Fig. 3). The damage induced by the implantation is maximized for temperatures of 20°C [Fig. 3(i)]. At the target implantation depth, ~1.1 μm, all the atoms in the crystal have been displaced (amorphization). As the implantation temperature increases, the crystal lattice damage goes down [Fig. 3(ii)–3(iv)]. The implant-induced damage reaches a minimum of 10 ppb for temperatures above 120°C [Fig. 3(iv)]. The reduction in implant damage is due to an increase in the diffusion of point defects, which leads to a reduction in amorphization [16]. Note that the region of the film with the highest density of defects is polished away in the final step of the smart-cut process.

In order to fabricate the waveguides in the SiC films, we deposit 1000 nm of plasma-enhanced chemical vapor deposition (PECVD) oxide hard mask and pattern the waveguides using e-beam lithography. The oxide hard mask and SiC layer are etched with fluorine chemistry in an inductively coupled reactive ion etcher. The gases used for etching the SiC film are trifluoromethane (CHF_3) and oxygen (O_2). The selectivity to the oxide hard mask is 0.9 with an etch rate of 100 nm/ min. We clad the waveguides by depositing 3 μm

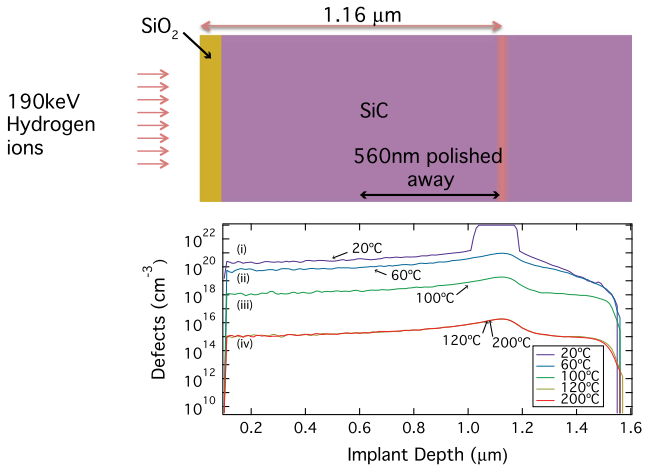

Fig. 3. Simulated hydrogen implantation-induced damage versus film depth. Note that for temperatures higher than 120°C, the induced implantation damage is at a minimum. We use a temperature of 200°C for our hydrogen implantation. After the film is sliced from the SiC wafer, it is 1.16 μm thick and we polish it down to 600 nm, where the crystal has minimal damage induced by the implantation.

of silicon oxide using PECVD. The waveguide is designed to ensure minimal overlap of the mode, with the possible defects introduced in the implantation step. The waveguide height is equal to the thickness of the SiC smart-cut film, 600 nm, and its width is 2700 nm [Fig. 3(b)]. The refractive index contrast is 1.15. The waveguide height and width are designed for anomalous dispersion at 2360 nm for the TE polarization. Note that most of the implanted defects are polished away when we thin the smart-cut SiC film from ~1.1 μm (as smart-cut) down to 600 nm.

We measure propagation losses of 7 dB/cm, only slightly more than a factor of two larger than the typical propagation loss of silicon-on-insulator [17]. Note that these losses are a factor of two to five lower than the loss obtained in epitaxial 3C SiC [12,13], which is mainly due to the quality of the material. The propagation loss is determined using the cutback method. We measure the power throughput of waveguides of 2.5, 4.6, and 7.3 mm in length, and calculate the change in power per unit length. We estimate these losses to not be fundamental: considering the defect density profile in Fig. 3, the measured losses are mostly due to the fabrication process still being in its infancy and originate due to a combination of scattering losses and losses due to residual defects in the crystal lattice. Scattering losses could be further minimized by optimizing the etching process and smoothing the sidewalls via oxidation, while residual defect losses could be minimized by annealing at higher temperatures.

Using the SiC-on-insulator platform we report, to our knowledge, the first demonstration of $\chi^{(3)}$-based nonlinear optics in SiC waveguides. In order to characterize the nonlinear coefficient n_2 for SiC, we measure the self-phase modulation (SPM) -induced spectral broadening by launching picosecond pulses into the waveguide and measuring the spectral output. In our experiment, we use an optical parametric oscillator (OPO) to generate 7.2 ps pulses centered at 2360 nm. The repetition rate of the OPO is 80 MHz. We couple the pulse train into an SiC waveguide using an aspheric lens. The coupling loss is 6 dB per facet. The output is collected using a lensed fiber and sent to an optical spectrum analyzer. The average power coupled to the waveguide is 167 mW, corresponding to a peak power of 280 W. The waveguide has a cross section of 600 nm × 2700 nm and is 7.3 mm long. Figure 4 shows the measured optical spectra for the input (black, dashed) and the waveguide output (red, solid). We observe spectral broadening by a factor of 1.93 due to the SPM in the waveguide.

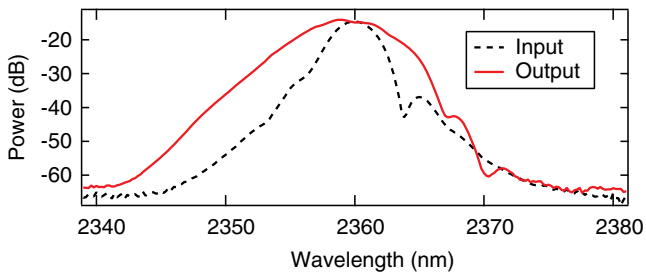

Fig. 4. Self-phase modulation in a 7.3 mm long, 600 nm × 2700 nm cross-section 4H silicon carbide waveguide. Measured optical spectra for input light (black, dashed) and broadened output light (red, solid).

We estimate the nonlinear refractive index for SiC extracted from the SPM measurements to be $n_2 = 8.6 \times 10^{-15}$ cm^2 W^{-1} at a wavelength of 2360 nm, which is comparable to that of silicon at the same wavelength [7]. The broadening factor β_{SPM} due to the SPM is given by $\beta_{\mathrm{SPM}} = 0.86\gamma P_{\mathrm{peak}} L_{\mathrm{eff}}$, where γ is the nonlinear parameter, P_{peak} is the peak pump power, and L_{eff} is the effective length of the medium, given by $L_{\mathrm{eff}} = [1 - \exp(-\alpha L)]/\alpha$ [18], and α is the propagation loss. The nonlinear refractive index is given by $n_2 = (\gamma c A_{\mathrm{eff}})/\omega_{\mathrm{pump}}$, where A_{eff} is the effective mode area of the waveguide. Based on the coupling and propagation losses, we characterize the nonlinear refractive index for three different waveguide lengths of 2.5, 4.6, and 7.3 mm, with measured broadening factors of 1.05, 1.31, and 1.93, respectively. We calculate a nonlinear refractive index $n_2 = 8.6 \pm 1.1 \times 10^{-15}$ cm^2 W^{-1}, which agrees well with the expected value of n_2 using Miller's Rule [19] and the van Stryland analysis [20]. The value of n_2 compares favorably to other CMOS-compatible materials: it is higher than silicon nitride, and is on the same order of magnitude as silicon. Note that in contrast to silicon, SiC does not suffer from two-photon absorption in the near-infrared region and longer wavelengths, and therefore offers promise as a platform for high-power nonlinear photonic devices.

In conclusion, we report the first demonstration of self-phase modulation in an SiC channel waveguide. We observe a broadening factor of 1.93 for a pump wavelength centered at 2360 nm. We measure a large third-order nonlinearity in silicon carbide, and show the potential of SiC as a platform for integrated nonlinear optical devices.

Funding. Defense Advanced Research Projects Agency (DARPA) (W911NF-11-1-0202); National Science Foundation (NSF) (ECCS-0335765).

Acknowledgment. The authors gratefully acknowledge support from DARPA for award no. W911NF-11-1-0202 supervised by Dr. Jamil Abo-Shaeer. This work was performed in part at the Cornell NanoScale Facility, a member of the National Nanotechnology Infrastructure Network, which is supported by the National Science Foundation (grant no. ECCS-0335765).

REFERENCES

1. M. A. Foster, A. C. Turner, M. Lipson, and A. L. Gaeta, Opt. Express **16**, 1300 (2008).
2. D. J. Moss, R. Morandotti, A. L. Gaeta, and M. Lipson, Nat. Photonics **7**, 597 (2013).
3. H. Jung, C. Xiong, K. Y. Fong, X. Zhang, and H. X. Tang, Opt. Lett. **38**, 2810 (2013).
4. B. J. M. Hausmann, I. Bulu, V. Venkataraman, P. Deotare, and M. Lončar, Nat. Photonics **8**, 369 (2014).
5. A. C. Turner, C. Manolatou, B. S. Schmidt, M. Lipson, M. A. Foster, J. E. Sharping, and A. L. Gaeta, Opt. Express **14**, 4357 (2006).
6. A. A. Borshch, M. S. Brodin, and V. I. Vokov, J. Exp. Theor. Phys. **45**, 490 (1977).
7. Q. Lin, J. Zhang, G. Piredda, R. W. Boyd, P. M. Fauchet, and G. P. Agrawal, Appl. Phys. Lett. **91**, 021111 (2007).
8. A. Vonsovici, G. T. Reed, and A. G. R. Evans, Mater. Sci. Semicond. Process. **3**, 367 (2000).
9. X. Tang, K. Wongchotigul, and M. G. Spencer, Appl. Phys. Lett. **58**, 917 (1991).
10. L. Di Cioccio, Y. Le Tiec, F. Letertre, C. Jaussaud, and M. Bruel, Electron. Lett. **32**, 1144 (1996).

11. S. Yamada, B.-S. Song, J. Upham, T. Asano, Y. Tanaka, and S. Noda, Opt. Express **20**, 14789 (2012).
12. X. Lu, J. Y. Lee, P. X.-L. Feng, and Q. Lin, Opt. Lett. **38**, 1304 (2013).
13. J. Cardenas, M. Zhang, C. T. Phare, S. Y. Shah, C. B. Poitras, B. Guha, and M. Lipson, Opt. Express **21**, 16882 (2013).
14. X. Song, J. F. Michaud, F. Cayrel, M. Zielinski, M. Portail, T. Chassagne, E. Collard, and D. Alquier, Appl. Phys. Lett. **96**, 142104 (2010).
15. Silvaco Athena (Silvaco International) www.silvaco.com.
16. W. Wesch, A. Heft, E. Wendler, T. BAchmann, and E. Glaser, Nucl. Instrum. Meth. B **96**, 335 (1995).
17. Y. Vlasov and S. McNab, Opt. Express **12**, 1622 (2004).
18. G. P. Agrawal, *Nonlinear Fiber Optics* (Academic, 2007).
19. C. C. Wang, Phys. Rev. B **2**, 2045 (1970).
20. M. Sheik-Bahae, D. C. Hutchings, D. J. Hagan, and E. W. Van Stryland, IEEE J. Quantum Electron. **27**, 1296 (1991).